

## PREPARATION AND PERFORMANCE TESTING OF $\text{WO}_3$ NANOFIBER PHOTOCATALYST BASED ON Cu DOPING

Xiangju HAN<sup>1,\*</sup>, Wenling YANG<sup>2</sup>

Currently, many scholars have proposed many photocatalysts to degrade pollutants in the air. However, numerous photocatalysts exhibit deficiencies in catalytic activity, heat resistance, pressure resistance, and resilience to heavy metal contamination. To address this issue, this study proposes a Cu-doped  $\text{WO}_3$  nanofiber photocatalyst to improve catalyst performance. The results of detecting the structure of the catalyst using relevant instruments showed that the catalyst could mix the diffraction peaks of Cu and  $\text{WO}_3$  materials, thereby improving the performance of the catalyst. The optical flow intensity of  $\text{WO}_3\text{-Cu}$  was on average  $1\text{mA/cm}^2$  higher than that of  $\text{WO}_3$  catalyst. The light absorption of the  $\text{WO}_3\text{-Cu}$  catalyst was much higher than that of the  $\text{WO}_3$  catalyst at wavelengths between 400nm-500nm and above 60nm. The main lattice spacing of the  $\text{WO}_3\text{-Cu}$  photocatalyst was 0.37nm, and the catalyst material was in close contact. The PL curve of  $\text{WO}_3\text{-Cu}$  was lower than that of Cu and  $\text{WO}_3$ , indicating that the  $\text{WO}_3\text{-Cu}$  catalyst had fewer defects. The catalyst was used in formaldehyde degradation experiments and found that the average degradation time of formaldehyde at different temperatures was 1.5 days. Under different pressure conditions, the average degradation time of formaldehyde by the catalyst was 2.3 days. Under different lighting conditions, the fastest decomposition rate of formaldehyde by the catalyst was 0.6g/h, and the catalyst's resistance to sulfur, mercury, and arsenic heavy metal toxicity reached 80%, 90%, and 95%, respectively. The working life of the catalyst could also reach 100%, fully meeting the expected requirements. The above results indicate that the proposed Cu-doped  $\text{WO}_3$  nanofiber photocatalyst can improve the catalytic efficiency and stability of the photocatalyst. This study provides a scientific basis for improving energy efficiency and reducing environmental pollution.

**Keywords:** Photocatalyst; Cu;  $\text{WO}_3$ ; Preparation; Performance testing; Catalytic speed

### 1. Introduction

The ongoing progression of industrialization has led to a marked increase in the emissions of mineral fuels, including coal, oil, and natural gas. This has resulted in a significant release of greenhouse gases and toxic substances into the atmosphere. The elevated energy consumption and emissions in industrial sectors have contributed to air and water contamination, thereby exerting a deleterious

<sup>1</sup> \* School of Engineering and Architecture, Henan Quality Polytechnic, Pingdingshan, China, corresponding author, e-mail: hanxiangju23@outlook.com

<sup>2</sup> Institute of Applied Engineering, Henan University of Science and Technology, Sanmenxia, China

effect on human health. Given this, many scholars have proposed using catalysts to degrade pollutants in the air <sup>[1]</sup>. However, there are currently many types of catalysts, among which catalysts that can utilize solar energy for catalytic action have shown great application prospects due to their low pollution and low cost <sup>[2]</sup>. Nanomaterial photocatalysts have the characteristics of high efficiency, multifunctionality, economy, and environmental friendliness. They exhibit superior catalytic efficiency and environmental adaptability, thereby leading to a significant reduction in the emission of harmful substances into the atmosphere and water bodies. Consequently, these systems contribute to a reduction in the cost and energy consumption associated with environmental governance.  $\text{WO}_3$  Nanofiber Photocatalyst ( $\text{WO}_3\text{NP}$ ) is currently a widely used photocatalyst <sup>[3]</sup>.  $\text{WO}_3$  nanofiber catalyst has high solar absorption efficiency and excellent photocatalytic efficiency, and its ability to degrade organic pollution also has important application value in environmental governance. Many scholars have researched it. For example, Li et al. designed a catalyst based on  $\text{WO}_3$  Nanofiber Materials ( $\text{WO}_3\text{NM}$ ) to improve the photocatalytic hydrogen production activity of composite catalysts. Compared with other catalysts, this catalyst increased the photocatalytic hydrogen production activity by 86.8% <sup>[4]</sup>. Cai et al. designed a novel photocatalyst based on  $\text{WO}_3\text{NM}$  to address the weak anti-toxicity ability of current catalysts. Compared with other catalysts, the anti-toxicity ability of this catalyst has been improved by 86.7% <sup>[5]</sup>. In addition, Li et al. prepared a  $\text{TiO}_2\text{-WO}_3$  photocatalyst to improve the degradation efficiency of indoor formaldehyde and tested it in indoor formaldehyde decomposition. The results showed that the catalyst could increase the degradation rate of formaldehyde by 9.5% <sup>[6]</sup>. Enesca et al. developed a  $\text{SnO}_2\text{-WO}_3$  heterojunction photocatalyst to address the low degradation efficiency of formaldehyde using a single  $\text{WO}_3$  catalyst. The catalyst was used in experiments for formaldehyde decomposition. The results showed that compared to the  $\text{WO}_3$  photocatalyst, the catalytic efficiency of the  $\text{SnO}_2\text{-WO}_3$  photocatalyst increased by 10.2% <sup>[7]</sup>. However, the quantum efficiency of the catalyst itself is low, the number of active sites indicated by the material is limited, and the recombination rate of electron hole pairs is high. Due to these reasons, the current  $\text{WO}_3$  photocatalyst still cannot meet the expected requirements in terms of catalytic speed and applicability <sup>[8]</sup>. Therefore, to accelerate the catalytic ability of  $\text{WO}_3$  catalysts and expand their applicability, it is necessary to optimize the current  $\text{WO}_3$  catalysts <sup>[9]</sup>. Doping Cu into  $\text{WO}_3\text{NM}$  can react with electrons in  $\text{WO}_3\text{NM}$ , promote charge separation, and effectively improve the redox performance of  $\text{WO}_3$  catalytic materials. This study utilizes Cu-doped  $\text{WO}_3\text{NP}$  ( $\text{WO}_3\text{-Cu}$ ) to degrade formaldehyde to test the performance of the catalyst and compare its differences with other catalysts. The innovative aspect of this study is the integration of  $\text{WO}_3\text{-Cu}$  and  $\text{WO}_3\text{NMs}$ , which utilizes the local electric field generated between guided  $\text{WO}_3$  photocatalysts in Cu dopants to facilitate charge separation. This enhances the photocatalytic efficiency

of  $\text{WO}_3$  photocatalysts, improves their heat resistance, stability, resistance to heavy metal pollution, and high voltage resistance.

## 2. Materials and Methods

### 2.1 Preparation of $\text{WO}_3\text{-Cu}$

#### 2.1.1 Characteristics and Application Status of $\text{WO}_3\text{NP}$

$\text{WO}_3$  nanowires are a unique semiconductor material. This material can be irradiated by a specific light source to oxidize nanoparticles attached to the medium with water in the environment and other gases in the air, producing extremely strong oxidation-reduction ability through oxidation [10]. It uses its oxidation-reduction ability to photodegrade and eliminate organic pollutants and some inorganic pollutants in the air or other environments, decomposing pollutants into harmless substances [11]. Moreover, the catalyst can also damage the cell wall of bacteria, thereby killing them. Therefore, this catalyst can not only decompose harmful substances but also play a role in sterilization [12]. This catalyst has a wide range of applications in energy fields such as chemical industry, environmental protection, color changing devices, sensors, photoelectrochemical devices, etc. [13]. The structural diagram of  $\text{WO}_3$  photocatalyst is shown in Fig. 1.

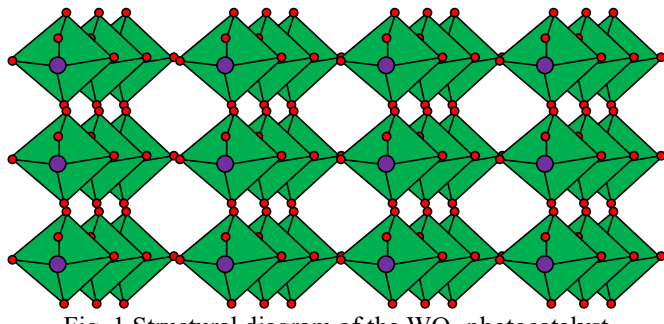


Fig. 1 Structural diagram of the  $\text{WO}_3$  photocatalyst

In Fig. 1, the  $\text{WO}_3$  photocatalyst is an orthogonal hexagonal close-packed structure, in which the W ions are located on the hexahedral coordination. This band structure can enhance the photocatalytic performance of  $\text{WO}_3$ . This catalyst can use the energy of light to excite the movement of electrons, thereby generating electron holes and binding active species on the surface of the object, thus achieving catalytic reactions.  $\text{WO}_3$  photocatalyst has excellent catalytic performance, especially outstanding performance in photocatalytic reactions. In wastewater treatment, this catalyst can generate redox pairs and promote the oxidative decomposition of organic matter in wastewater under the action of light. Therefore, it can reduce the content of organic matter in wastewater and minimize environmental pollution. In other fields,  $\text{WO}_3$  photocatalysts can also utilize their redox reactions to increase reaction rates and decompose pollutants. In summary,

WO<sub>3</sub>NP has excellent catalytic performance in electronic structure design and has broad application prospects. However, currently, the photocatalytic efficiency of WO<sub>3</sub>NP is relatively low, so it is necessary to find a way to improve the photocatalytic efficiency of this catalyst. Cu doping is used to guide the formation of local electric fields between WO<sub>3</sub> photocatalysts, thereby achieving charge separation and improving the photocatalytic efficiency of WO<sub>3</sub> photocatalysts.

### 2.1.2 Preparation Method of WO<sub>3</sub>-Cu

WO<sub>3</sub>-Cu is widely used as an efficient catalyst in various fields [14-15]. The preparation method is shown in Fig. 2.

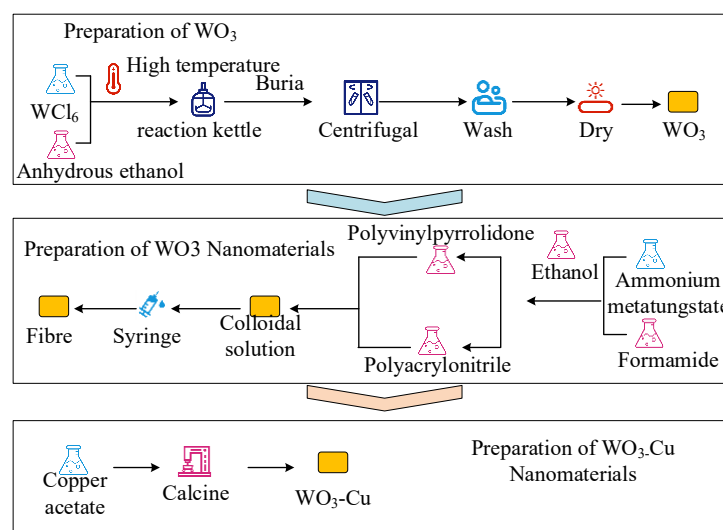


Fig. 2 The WO<sub>3</sub>-Cu preparation method

In Fig. 2, the preparation method of WO<sub>3</sub>-Cu is divided into three steps: the preparation of WO<sub>3</sub>, the preparation of WO<sub>3</sub> nanofibers, and the doping of Cu into WO<sub>3</sub> nanofibers. Among them, the preparation method of WO<sub>3</sub> is to disperse WCl<sub>6</sub> in ethanol without water molecules and mix them. Then, under high-temperature conditions of 180 degrees, the mixture is transferred to a reaction vessel for chemical reaction. After 24 hours, the reaction stops and the reactants are cooled. After cooling, centrifugation is performed to remove the liquid and obtain a precipitate, which is then washed with deionized water and ethanol. Finally, the washed object is dried to remove excess moisture and obtain a WO<sub>3</sub> solid. Then, the prepared WO<sub>3</sub> solid and electrospinning method is used to prepare WO<sub>3</sub> nanofibers. When preparing nanofibers, it is necessary to first prepare a spinning solution under normal temperature and pressure conditions. When preparing the spinning solution, ammonium meta-tungstate needs to be dissolved in formamide, and an appropriate amount of ethanol needs to be added to adjust the volatility and

viscosity of the solution. After the solution is mixed evenly, polyvinylpyrrolidone and polyacrylonitrile need to be added and stirred to obtain a transparent gel-like solution. The syringe is reused to form fibers from the transparent solution. Finally, the preparation of the  $\text{WO}_3\text{-Cu}$  catalyst is carried out. Subsequently, an appropriate amount of copper acetate is added to the  $\text{WO}_3\text{-NM}$  solution, and the solution is calcined at high temperature in a calcination furnace to obtain  $\text{WO}_3\text{-Cu}$ . After the material is prepared, the crystal diffraction peaks of the material are recorded using X-ray diffraction, and the structure of the material is detected using an accelerated electric field. The spectrometer is reused to analyze the visible light absorption ability of the photocatalyst. The calculation method for the light absorption capacity of the catalyst is shown in equation (1).

$$(\lambda h\nu)^{\frac{1}{n}} = a(h\nu - w) \quad (1)$$

In equation (1),  $\lambda$  is the material absorption coefficient.  $h\nu$  is the energy of photons.  $n$  is the indirect bandgap of the material.  $a$  is a constant.  $\nu$  is the frequency of the incident light.  $h$  is Planck's constant.  $w$  is the bandgap of the material.

### 2.1.3 Preparation Reagents and Instruments for Cu-doped $\text{WO}_3$ photocatalyst

To prepare  $\text{WO}_3\text{-Cu}$  material, the reagents used in the experiment are listed in Table 1.

Table 1

Experimental reagents

Reagent name	Reagent source	Characteristic	Reagent name	Reagent source	Characteristic
99.9% $\text{WCl}_6$	Shanghai Aladdin Biochemical Technology Co., Ltd	Inorganic compounds with relatively stable chemical properties	$\text{C}_2\text{H}_5\text{OH}$ , 80%	Shanghai Aladdin Biochemical Technology Co., Ltd	Colorless, transparent, volatile, and flammable liquid
$\text{C}_2\text{H}_5\text{OH}$ , 99.7%	Xilong Chemical Co., LTD	Colorless and transparent liquid, flammable, esterification reaction	Polyvinyl pyrrolidone	Xilong Chemical Co., LTD	White or almost white powder, easy to flow
$(\text{CH}_3\text{COO})_2\text{Zn}$ , 99.0%	Tianjin Bodhi Chemical Co., Ltd	Hexahedral scales react with strong oxidants	Polyacrylonitrile	Shanghai Aladdin Biochemical Technology Co., Ltd	White powder
Ammonium meta tungstate	Shanghai Aladdin Biochemical	White rhombohedral crystal, insoluble in	$\text{Cu}(\text{CH}_3\text{COO})_2$	Xilong Chemical Co., LTD	Inorganic salt compounds

	Technology Co., Ltd	alcohol substances			
DMF	Shanghai Aladdin Biochemical Technology Co., Ltd	Colorless and transparent liquid, not easily oxidized or reduced	Absolute ethyl alcohol	Shanghai Aladdin Biochemical Technology Co., Ltd	Colorless and transparent liquid, with a special fragrance, easily volatile

In addition, many experimental instruments are also used in material preparation. The instrument and instrument model configuration used in the experiment are as follows: the JDF-04 electrospinning machine from Changsha Nayi Instrument Technology Co., Ltd. is used to synthesize  $\text{WO}_3\text{NM}$ . The TL1200 tube furnace from Nanjing Boyuntang Instrument Technology Co., Ltd. is used for material calcination. The DHG-9070A blast drying oven from Shanghai Jinghong Experimental Equipment Co., Ltd. is used for material drying operations. After the preparation of the reagent is completed, the characterization ability of the catalyst material needs to be tested. During the testing process, it is necessary to use the D8 ADVANCE X-ray diffractometer from the German company BRUKER to record the diffraction peaks of the catalyst crystal plane and the electron binding energy of the catalyst and detect the crystal structure of the catalyst. The surface area and pore volume of the catalyst are calculated using the BET-specific surface area of the NOVA Quanta Chrome 1000e model from Kantar Instruments in the United States. Ultraviolet visible diffuse reflectance spectroscopy is used to record the visible light absorption ability of photocatalysts. Finally, it is necessary to use electron paramagnetic resonance to detect the strength of the free radical generation signal of the catalyst.

## 2.2 Application of Cu-doped $\text{WO}_3$ Photocatalyst in the Degradation of Formaldehyde

### 2.2.1 Application Principle

To solve the problem of difficult complete degradation of formaldehyde in indoor gases, many scholars have proposed using  $\text{WO}_3$  photocatalysts for formaldehyde degradation [16-17]. The unique nanowire structure of  $\text{WO}_3$  photocatalyst can effectively capture formaldehyde molecules in the air. The built-in electric field formed by Cu and  $\text{WO}_3$  in  $\text{WO}_3\text{-Cu}$  can effectively drive the separation of photo generated electron pairs, thereby generating a large amount of active free radicals and utilizing them to degrade formaldehyde. The principle of  $\text{WO}_3\text{-Cu}$  for formaldehyde degradation is shown in Fig. 3.

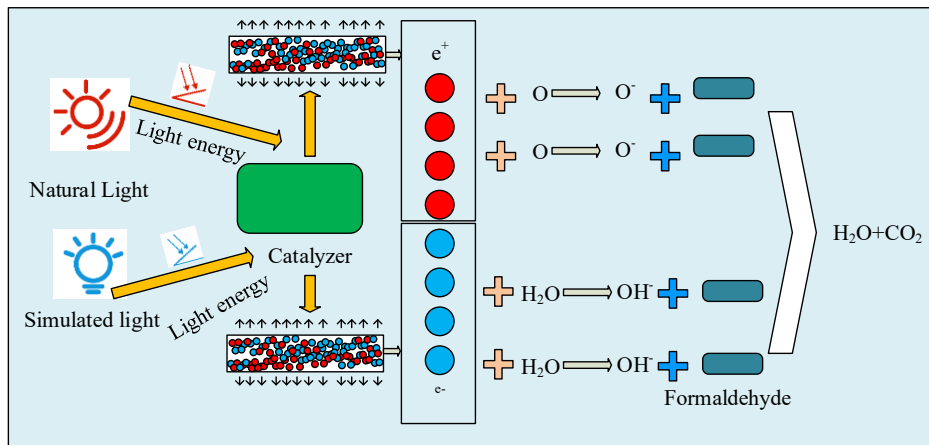


Fig. 3 Application principle of catalyst for formaldehyde degradation

In Fig. 3, when the  $\text{WO}_3$ -Cu catalyst degrades formaldehyde, the catalyst adsorbs formaldehyde molecules onto the surface through its own pore structure. Then, under specific lighting conditions, the photocatalyst will absorb light energy, and the electrons in the catalyst will move due to energy changes. This movement process is called the electron transition phenomenon. In the phenomenon of electronic transition, there are positive and negative electrons. Electrons with negative charges combine with oxygen in the air to form negative oxygen ions. Positively charged holes combine with water in the air to generate hydroxyl radicals. The chemical properties of the objects generated by these combinations are extremely unstable. When the substance comes into contact with the organic compound formaldehyde adsorbed on the catalyst surface, a strong chemical reaction occurs. Formaldehyde molecules undergo redox reactions under the action of catalysts. During the catalytic oxidation process, formaldehyde molecules combine with hydroxyl radicals and negative oxygen ions generated in the catalyst, resulting in the formation of water and carbon dioxide, effectively removing formaldehyde molecules. Subsequently, the produced water and carbon dioxide become detached from the surface of the catalyst, thereby completing the formaldehyde degradation process. During the degradation process of formaldehyde, the chemical reaction of formaldehyde cracking into formic acid is shown in equation (2).



After formaldehyde is cracked into formic acid, formic acid undergoes further cracking reaction, as shown in equation (3).



Through the above reaction, formaldehyde is degraded into environmentally friendly water molecules and carbon dioxide. Afterwards, the high formaldehyde content in the air is detected and calculated to determine whether it can meet the

degradation standards. The calculation method for formaldehyde concentration in the air is shown in equation (4).

$$\rho = R / V \quad (4)$$

In equation (4),  $\rho$  is the formaldehyde concentration,  $R$  is the formaldehyde detection result, and  $V$  is the air volume.

### 2.2.2 Experimental Materials and Instruments

When conducting experiments on the degradation of formaldehyde based on  $\text{WO}_3\text{-Cu}$ , the first step is to prepare the formaldehyde reagent. Table 2 shows the reagents and their sources required for formaldehyde preparation.

Table 2  
Experimental reagents

Reagent name	Reagent source	Characteristic	Reagent name	Reagent source	Characteristic
NaOH	Shanghai Aladdin Biochemical Technology Co., Ltd	White semi transparent crystalline solid, easily soluble in water	Sorbic alcohol	Tianjin Bodi Chemical Co., Ltd	White crystalline powder, odorless, hygroscopic
Sal perlatum	Xilong Chemical Co., LTD	White crystalline or crystalline powder, odorless, easily soluble in water	Ethanedi ol	Tianjin Bodi Chemical Co., Ltd	Colorless, odorless, and sweet viscous liquid
Disodium hydrogen phosphate dodecamolecular water	Tianjin Bodi Chemical Co., Ltd	Colorless translucent crystal or white crystalline powder	Propanetriol	Tianjin Bodi Chemical Co., Ltd	Colorless, odorless, and sweet viscous liquid
Sodium dihydrogen phosphate dimolecul ar water	Tianjin Bodi Chemical Co., Ltd	Colorless crystal, highly soluble in water, but prone to clumping in humid air	Fatty alcohol-polyoxy ethylene ether	Shanghai Aladdin Biochemical Technology Co., Ltd	Easy to dissolve in water and various organic solvents, with high stability
Poly (vinyl acetal)	Tianjin Bodi Chemical Co., Ltd	Microstrip grass yellow solid, thermoplastic, density 1.2	Stearic acid polyether fat	Tianjin Bodi Chemical Co., Ltd	Milky white solid at 25 °C
Phenol reagent	Tianjin Bodi Chemical Co., Ltd	White to pale yellow powder, soluble in water, slightly soluble in anhydrous ethanol, insoluble in ether	Ammonium ferric sulfate; ferriam monium sulfate;	Tianjin Bodi Chemical Co., Ltd	Colorless octahedral crystal with a density of 1.71 g/cm <sup>3</sup> and a melting point between 39 and 41 °C

The formaldehyde reagent prepared based on the above reagents is used for

formaldehyde degradation experiments. Instrument name and model during the experiment: First, a xenon lamp is used to simulate sunlight to irradiate the catalyst, and a mercury lamp is used to simulate ultraviolet light to test the degradation rate. Next, the incident light energy is measured using an optical power meter to control the magnitude of the incident light energy. It is necessary to use filters to filter out useless light. The experiment needs to be conducted in a light shield to avoid the influence of external light on the experimental results. The entire experiment will be conducted in a quartz reactor. At the end of the experiment, the formaldehyde content is detected using a gas chromatograph and formaldehyde reagent kit. The experiment of photocatalytic degradation of formaldehyde is conducted based on the above reagents and instruments.

### 2.2.3 Experimental Methods

Based on the  $\text{WO}_3$ -Cu, it is a reagent with strong redox reactions that can be used for the purification of polluted gases in the air. This study utilizes the catalyst to purify formaldehyde in the air and tests its performance, as shown in Fig. 4.

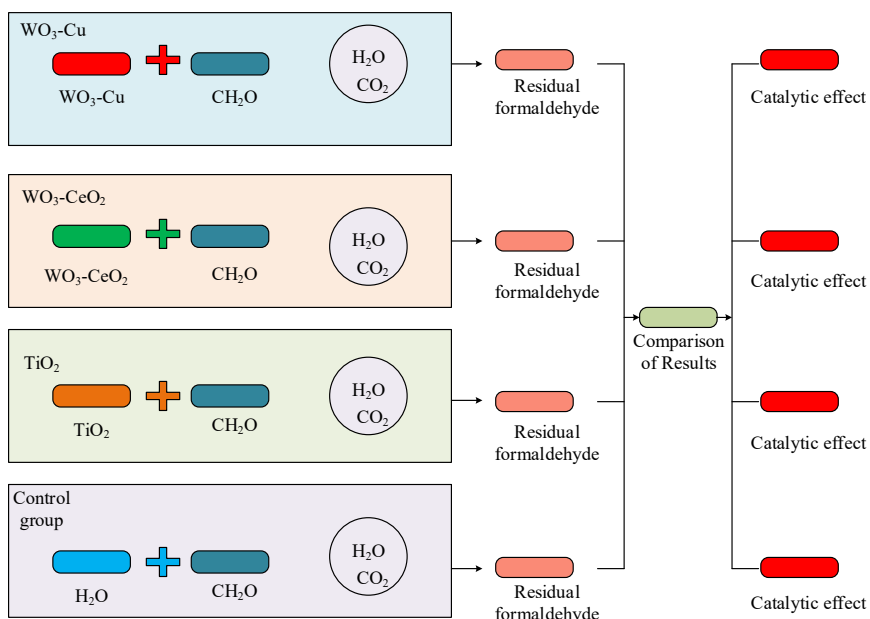


Fig. 4 Experimental Methods

In Fig. 4, there are four groups in the experiment. One group of catalysts is based on  $\text{WO}_3$ -Cu, one group is a  $\text{WO}_3$ - $\text{CeO}_2$  heterojunction photocatalyst, one group is a titanium dioxide catalyst, and the last group without a catalyst is used as a control group. During the experiment, the formaldehyde content is controlled to be consistent across all four groups, and the catalyst quality and quantity are held constant. Pure water with the same catalyst quantity as the first three groups is

added to the control group without a catalyst to meet the requirements of controlling variables. After fully reacting formaldehyde with the catalyst and purified water, a formaldehyde reagent kit is used to test the remaining formaldehyde content and compare the test results. The formaldehyde content after catalytic degradation in the experiment is measured at different temperatures and times, and the results of the four tests are compared. Based on this comparison, the catalytic performance of  $\text{WO}_3\text{-Cu}$  is analyzed.

### 3. Results

#### 3.1 Analysis of Preparation Results of $\text{WO}_3\text{-Cu}$

To verify the preparation results of  $\text{WO}_3\text{-Cu}$ , this study uses an X-ray diffractometer to examine the diffraction peaks of the catalyst crystal plane. The results of comparing the crystal structures are shown in Fig. 5.

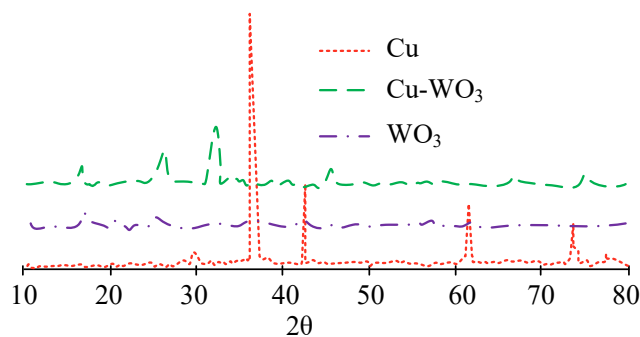
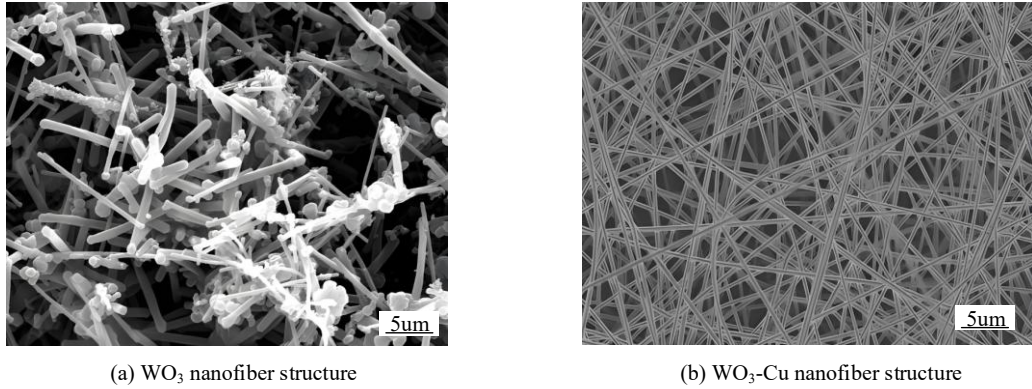
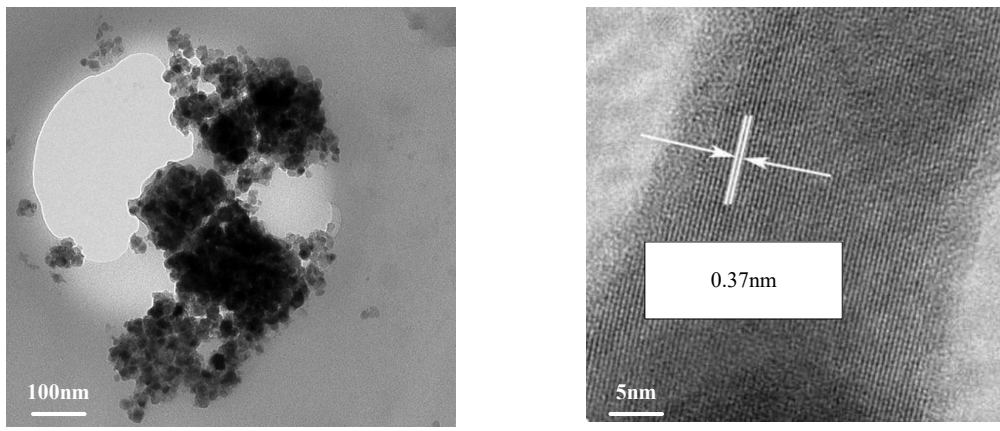


Fig. 5 Cu and  $\text{WO}_3$  diffraction profiles

From Fig. 5, the peak of the  $\text{WO}_3$  diffraction peak is enhanced after recombination, while a few peaks of Cu are weakened compared to before, but most peaks are enhanced. This result indicates that after the composite of  $\text{WO}_3$  and Cu, the crystal structure rate of the catalyst changes, and the crystallinity of the catalyst increases compared to before. Conversely, during the composite process, the particles of the composite material undergo elongation, leading to the aggregation of smaller particles and the formation of larger particles. This phenomenon results in an increase in XRD diffraction peaks. This also increases the contact area between the catalyst and the substance, which is beneficial for catalytic reactions. Further Scanning Electron Microscopy (SEM) image comparison is conducted on the morphology characteristics of the prepared catalyst, and the results are shown in Fig. 6.

Fig. 6 SEM images of  $\text{WO}_3$  and  $\text{WO}_3$ -Cu

In Fig. 6 (a), the individual  $\text{WO}_3$  fiber material is composed of a large number of nanoparticles, and the surface of these nanoparticles is rough. When they come into contact with other substances in the air, they immediately undergo chemical reactions, which can increase the catalytic effect with the catalyst. In Fig. 6 (b), the  $\text{WO}_3$ -Cu photocatalyst is also composed of a large number of nanofibers, and the diameter of the  $\text{WO}_3$ -Cu nanofibers is smaller than that of the  $\text{WO}_3$  fiber material alone. Therefore,  $\text{WO}_3$ -Cu materials have a larger surface area and are more able to come into contact with external substances, thereby improving the catalytic rate of the catalyst. The Transmission Electron Microscopy (TEM) image of  $\text{WO}_3$ -Cu is shown in Fig. 7.

(a) TEM image of  $\text{WO}_3$ -Cu at 100nm(b) TEM image of  $\text{WO}_3$ -Cu at 5nmFig. 7 The TEM plot of  $\text{WO}_3$ -Cu

In Fig. 7 (a), the distribution of various particles in  $\text{WO}_3$ -Cu material cannot be separated from the majority of Cu particles in  $\text{WO}_3$  nanosheets. The high-resolution electron microscopy image in Fig. 7 (b) shows that  $\text{WO}_3$  and Cu have

high crystallinity. After measurement, the main lattice spacing of  $\text{WO}_3$ -Cu is 0.37nm. It can be inferred from the tightness of the contact surface of the material that a heterojunction is formed after the composite of  $\text{WO}_3$  and Cu material. This can accelerate the charge transfer between the catalyst and the carrier, enhancing the catalytic effect. Further analysis of the UV-Vis spectra of  $\text{WO}_3$ -Cu, Cu, and  $\text{WO}_3$  is shown in Fig. 8.

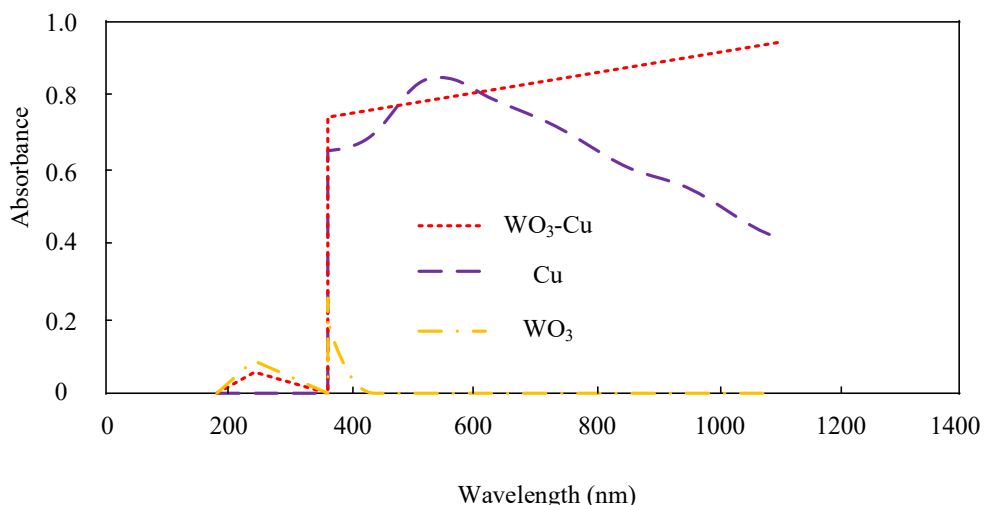


Fig. 8 The UV-Vis spectra of  $\text{WO}_3$ , Cu, and  $\text{WO}_3$ -Cu

According to Fig. 8, the light absorption of  $\text{WO}_3$ -Cu catalyst in the visible light range of 400nm-500nm is higher than that of Cu and  $\text{WO}_3$ . After the wavelength is greater than 600nm, the visible light absorption of  $\text{WO}_3$ -Cu catalyst is higher than that of  $\text{WO}_3$  and Cu materials. According to this experiment,  $\text{WO}_3$ -Cu material can improve the two-point visible light catalytic performance of  $\text{WO}_3$  material. Further analysis is conducted on the Energy Dispersive X-ray Detector (EDX) image of the material, and the results are shown in Fig. 9.

The EDX test is conducted on the prepared  $\text{WO}_3$ -Cu material. In Fig. 9, there are only three elements (W, O, and Cu) in the prepared sample, which proves that the prepared  $\text{WO}_3$ -Cu material has no other molecules, atoms, or ions present. Besides, the prepared  $\text{WO}_3$ -Cu material is pure. Finally, the PL spectrum of the material is analyzed, and the results are shown in Fig. 10.

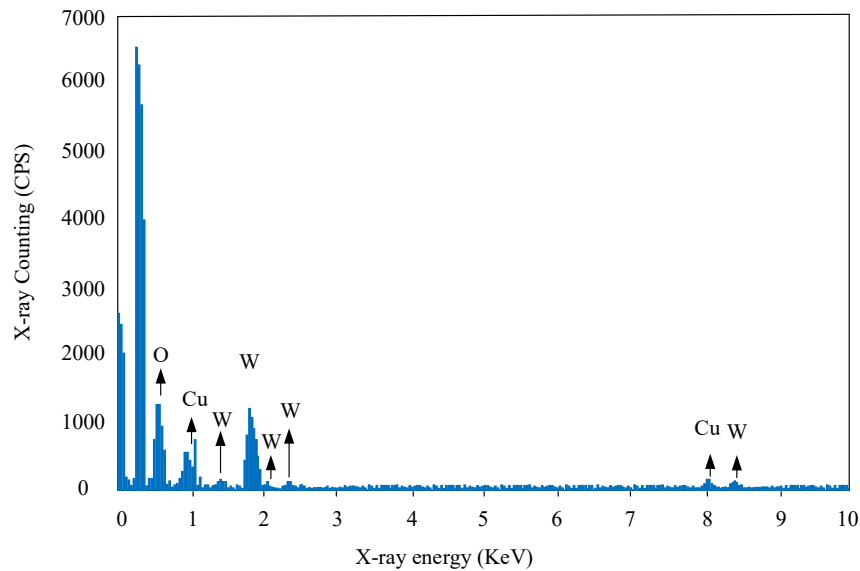
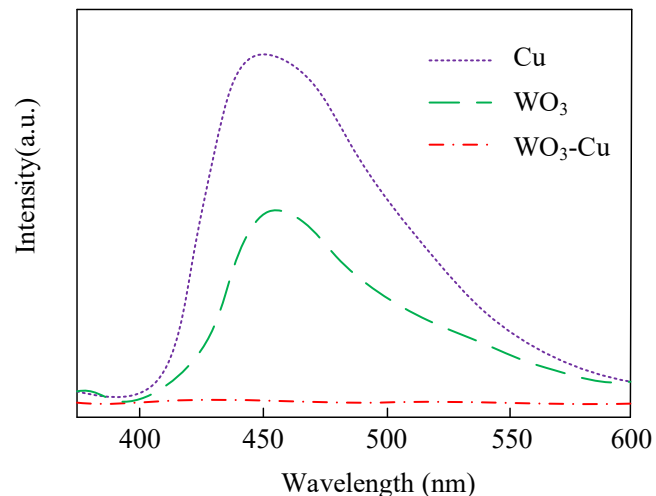
Fig. 9 The EDX image of  $\text{WO}_3$ -Cu

Fig. 10 PL spectral analysis of materials

As shown in Fig. 10, the PL curve of  $\text{WO}_3$ -Cu material is much lower than that of Cu material and  $\text{WO}_3$ . This result indicates that the fewer defects in the  $\text{WO}_3$ -Cu catalyst, the higher the efficiency of charge separation during catalytic reaction. Fig. 11 shows the photoelectric performance test of the prepared catalyst.

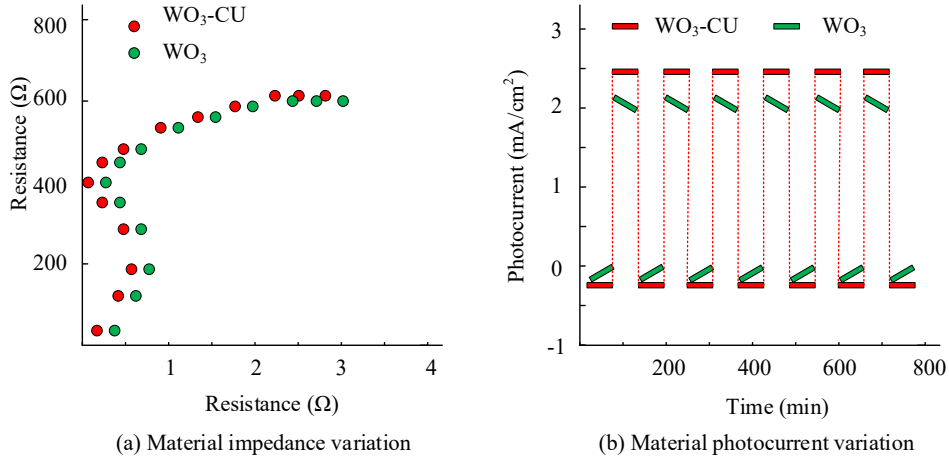


Fig. 11 Impedance and photocurrent changes of the prepared material

The impedance and photocurrent changes of materials can represent the photoelectric conversion performance of catalysts. In Fig. 11 (a), if the impedance of  $\text{WO}_3$ -Cu is low, the electrons on the surface of the material are prone to transition and migration separation after being excited by light, making it easier to catalyze. In Fig. 11 (b), the photocurrent intensity of  $\text{WO}_3$ -Cu is much higher than that of  $\text{WO}_3$  material alone, and the photocurrent intensity of  $\text{WO}_3$ -Cu photocatalyst changes relatively steadily. The higher the photocurrent intensity, the more mobile electron pairs the catalyst generates under photoexcitation, and the stronger the catalytic effect. The above detection results indicate that  $\text{WO}_3$ NP based on Cu doping has the same catalytic performance as other catalysts.

### 3.2 Analysis of Catalyst Application Results

After analyzing the results of the prepared  $\text{WO}_3$ -Cu, a comparison is made between the degradation changes of  $\text{WO}_3$ -Cu,  $\text{WO}_3$ - $\text{CeO}_2$ , titanium dioxide catalyst, and formaldehyde without catalyst at different temperatures and pressures, as shown in Fig. 12.

In Fig. 12 (a), at any temperature,  $\text{WO}_3$ -Cu has the shortest degradation time and the best catalytic effect for formaldehyde. The catalyst takes an average of 1.5 days to degrade formaldehyde, and the degradation time of formaldehyde decreases with increasing temperature, but the change is not significant. The temperature has little effect on the catalyst.  $\text{WO}_3$ - $\text{CeO}_2$  and  $\text{TiO}_2$  catalysts have a strong dependence on temperature, and as the temperature increases, the degradation time first decreases and then increases.

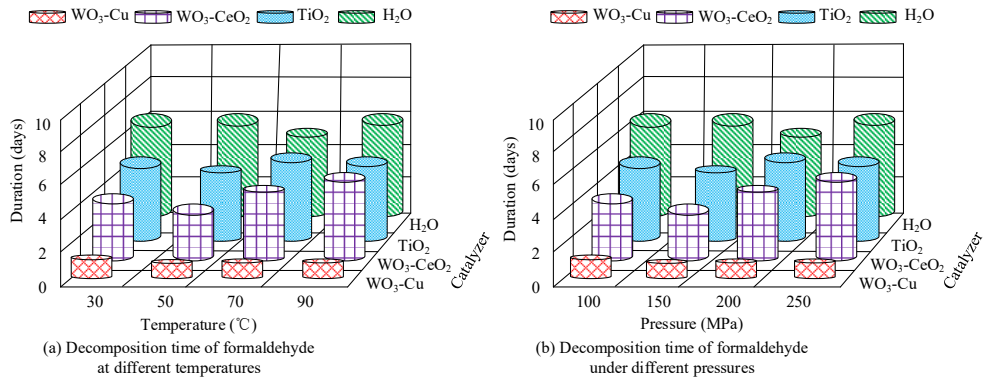


Fig. 12 Time-consuming for the catalyst to degrade formaldehyde

In Fig. 12 (b), as the pressure increases, the degradation time of formaldehyde by  $\text{WO}_3\text{-Cu}$  remains basically unchanged at around 2.3 days. The degradation time of formaldehyde by other catalysts first decreases with increasing pressure, and then increases with increasing pressure, that is, the degradation rate first increases and then decreases. The average degradation time of  $\text{WO}_3\text{-CeO}_2$  is 6.8 days, while the degradation time of  $\text{TiO}_2$  catalyst is 8.7 days. The above experimental results show that the prepared  $\text{WO}_3\text{-Cu}$  photocatalyst has low impurity content, stable catalyst structure, and good matching with the absorption spectrum of formaldehyde. Therefore, it can rapidly degrade formaldehyde and save degradation time. The performance of  $\text{WO}_3\text{-Cu}$  photocatalyst is compared with Degussa P25,  $\text{TiO}_2$  catalyst, and corresponding  $\text{TiO}_2\text{-WO}_3$  photocatalyst and  $\text{SnO}_2\text{-WO}_3$  photocatalyst in the reference. The results are shown in Table 3.

Table 3

#### Performance comparison of photocatalysts

Catalyst type	Catalyst activity	Light absorption	Photogenerated charge separation efficiency	Solar conversion efficiency
Degussa P25	81.2%	>400nm	82.1%	81.4%
$\text{TiO}_2$	78.1%	280-400nm	79.4%	80.4%
$\text{TiO}_2\text{-WO}_3$	80.3%	400~780nm	80.4%	83.4%
$\text{SnO}_2\text{-WO}_3$	83.7%	400~780nm	82.3%	82.4%
$\text{WO}_3\text{-Cu}$	89.2%	>200nm	88.4%	89.7%

The catalytic activity of photocatalysts is expressed in terms of conversion rate, which refers to the percentage of a certain reactant consumed in the reaction compared to the total amount of the original reactant. According to Table 3, the catalyst activity of the proposed  $\text{WO}_3\text{-Cu}$  photocatalyst is 89.2%, which is higher than other current photocatalysts. The imaging charge separation efficiency and solar energy conversion efficiency of  $\text{WO}_3\text{-Cu}$  photocatalyst are superior to other

photocatalysts. The superior performance of the  $\text{WO}_3\text{-Cu}$  photocatalyst relative to other catalysts can be attributed to the induced generation of a high number of active free radicals by light in the  $\text{WO}_3\text{-Cu}$  catalyst. In contrast, the number of active free radicals in other catalysts is lower than that in the  $\text{WO}_3\text{-Cu}$  photocatalyst, resulting in lower performance of the former relative to the latter. Fig. 13 compares the catalytic rates of various catalysts for formaldehyde degradation under different impact forces and light intensities.

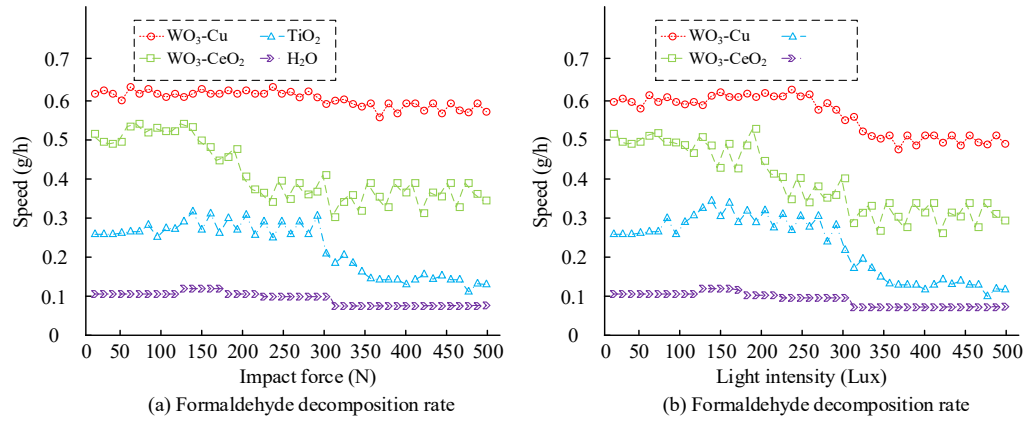


Fig. 13 Comparison of formaldehyde decomposition speed

In Fig. 13 (a), under different impact forces,  $\text{WO}_3\text{-Cu}$  has the fastest decomposition rate of formaldehyde, with an average rate of 0.6g/h. The decomposition rate of formaldehyde remains basically unchanged with the increase of impact force. The degradation rate of formaldehyde by  $\text{WO}_3\text{-CeO}_2$  varies greatly with the impact force. When the impact force reaches 150N, the decomposition rate reaches its maximum value of 0.57g/h. However, when the impact force exceeds 150N, the catalyst's decomposition rate of formaldehyde decreases. The decomposition rate of formaldehyde by  $\text{TiO}_2$  catalyst shows the same trend as that of  $\text{WO}_3\text{-CeO}_2$ , but its highest decomposition rate reaches 0.31g/h at an impact force of 100N and continues to decrease thereafter. In Fig. 13 (b), the decomposition rate of formaldehyde by the catalyst first increases with the increase of light intensity, and after exceeding the critical value, it will decrease with the increase of light intensity. The elevated catalytic rate exhibited by the  $\text{WO}_3\text{-Cu}$  photocatalyst in comparison to alternative photocatalysts under varying impact forces and light intensities can be attributed to its structural stability, which renders it relatively impervious to external perturbations. Consequently, the  $\text{WO}_3\text{-Cu}$  photocatalyst demonstrates a heightened catalytic stability, a property that sets it apart from other photocatalysts. Table 4 compares the degradation rate of formaldehyde by catalysts with different toxicities and the lifespan of the catalysts during operation.

Table 4  
**Antitoxicity and longevity of the catalyst**

Catalyst type	Antitoxicity						Working life (days)	Degradation time (days)
	S	Standard	Hg	Standard	As	Standard		
$\text{WO}_3\text{-Cu}$ phstocatalyzer	80%	70%	90 %	80%	95%	80%	2	2
$\text{WO}_3\text{-CeO}_2$ phstocatalyzer	70%	70%	75 %	80%	70%	80%	3	5
$\text{TiO}_2$ catalyst	64%	70%	70 %	80%	74%	80%	4	8
$\text{H}_2\text{O}$	60%	70%	60 %	80%	60%	80%	10	10

In Table 4, among several catalysts,  $\text{WO}_3\text{-Cu}$  can achieve the expected standard of anti-toxicity to various heavy metals. The toxicity resistance of  $\text{WO}_3\text{-CeO}_2$  and  $\text{TiO}_2$  catalysts to the three heavy metals does not meet the expected standards. Moreover, the working life of  $\text{WO}_3\text{-Cu}$  has reached 100%, which means it can work from formaldehyde degradation until formaldehyde degradation is complete. The working life of  $\text{WO}_3\text{-CeO}_2$  is only 60% and the catalyst stops working before formaldehyde is completely degraded. The working life of  $\text{TiO}_2$  catalyst is lower, only 50%. The above experiments indicate that  $\text{WO}_3\text{-Cu}$  has a faster catalytic rate, stronger adaptability to temperature, pressure, impact force, and light intensity, and wider applicability. Its anti-toxicity ability and service life are also the strongest among catalysts.

#### 4. Discussion

To test the performance of  $\text{WO}_3\text{-Cu}$ , the study first prepared the  $\text{WO}_3\text{-Cu}$  catalyst and analyzed the characterization results of the prepared catalyst. The results showed that the prepared  $\text{WO}_3\text{-Cu}$  catalyst material had a larger surface area and volume, and the  $\text{WO}_3\text{-Cu}$  material was prone to form heterojunction structures, which could accelerate the catalytic reaction rate of the catalyst. Further analysis of XRD data, UV-Vis, PL, and EDX images of the prepared  $\text{WO}_3\text{-Cu}$  catalyst showed that the crystallinity of the catalyst was improved compared to  $\text{WO}_3$  and Cu, and the absorption of visible light was also increased. Moreover, the PL curve of the catalyst was much lower than that of Cu and  $\text{WO}_3$ . The results indicate that the prepared  $\text{WO}_3\text{-Cu}$  catalyst has a larger surface area, more efficient photocatalytic performance, and higher charge separation efficiency, thereby improving the reaction efficiency of the catalyst during catalytic reactions. After that, this study compared the catalyst with the  $\text{WO}_3\text{-CeO}_2$  photocatalyst and  $\text{TiO}_2$  catalyst. Under different conditions, the degradation effect of three catalysts on formaldehyde was tested to evaluate the performance of the photocatalyst. Experiments have shown that under the same conditions, the average degradation time of formaldehyde by  $\text{WO}_3\text{-Cu}$  was 1.5 days with temperature changes, and the degradation time of the catalyst did not change significantly with increasing temperature. The degradation of formaldehyde by  $\text{WO}_3\text{-CeO}_2$  and  $\text{TiO}_2$  took 6.5 and 9.7 days, respectively, and

was greatly affected by temperature. This result was similar to the experimental results of Quyen et al.'s research. The reason for this result may be that the crystal surface structure of the  $\text{WO}_3$ -Cu photocatalyst has changed, which increases the heat resistance of the photocatalyst and improves its performance <sup>[18]</sup>. In addition, the degradation rate of formaldehyde by catalysts under different impact forces was compared. Under different impact forces, the degradation rate of formaldehyde by  $\text{WO}_3$ -Cu photocatalyst remained almost unchanged at 0.57g/h, while other catalysts first increased their degradation rate with the increase of impact force. After reaching the critical value, the degradation rate would decrease with the increase of impact force, and the degradation rate was extremely unstable, resulting in a poor catalytic effect of the catalyst. This result was consistent with the conclusion of Badour et al. However, in the experiments of Cu-doped and undoped  $\text{WO}_3$  photochromic films, the catalytic effect of  $\text{WO}_3$ -Cu was lower than that in this experiment. The reason might be that Badour's team did not test the prepared  $\text{WO}_3$ -Cu material during the experiment, resulting in the presence of many impurities in the photocatalyst, which seriously affected the catalytic effect <sup>[19]</sup>. This study also conducted experiments on the anti-toxicity ability and service life of concentrated catalysts. The anti-toxicity ability of  $\text{WO}_3$ -Cu photocatalyst towards heavy metals such as sulfur, mercury, and arsenic could meet the expected standards. The anti-toxicity performance of  $\text{WO}_3$ - $\text{CeO}_2$  towards mercury and arsenic did not meet the expected requirements, while the anti-toxicity performance of  $\text{TiO}_2$  towards the three heavy metals did not meet the expected standards. From the perspective of working life,  $\text{WO}_3$ -Cu could play a role in the entire process of formaldehyde degradation, while  $\text{WO}_3$ - $\text{CeO}_2$  had a working life of only 60% and  $\text{TiO}_2$  had a working life of only 50% in the formaldehyde degradation process. This result was similar to the experimental results of Qi et al. This is because  $\text{WO}_3$ NP doped with Cu ions could alter the activity of  $\text{WO}_3$ , causing it to continuously react with formaldehyde and generate positive and negative electrons. Thus, it could continuously undergo redox reactions with formaldehyde until formaldehyde was completely degraded <sup>[20]</sup>.

Experimental data show that the proposed  $\text{WO}_3$ -Cu can change the crystal structure of  $\text{WO}_3$  material, thereby improving the catalytic effect of the catalyst at high-temperature and high-pressure, and ensuring the activity of the catalyst. Moreover, by changing the internal structure of  $\text{WO}_3$ , the anti-toxicity performance and working life of the photocatalyst have been improved. Therefore,  $\text{WO}_3$ -Cu photocatalyst has excellent heat resistance, stability, resistance to heavy metal pollution, and high pressure resistance.

## 5. Conclusion

In response to the current unsatisfactory catalytic effect, low catalytic activity, and weak stability of photocatalysts, this study proposed a  $\text{WO}_3$ -Cu

catalyst to improve the catalytic efficiency of traditional photocatalysts. The present study initiated with the introduction of a novel preparation method for the catalyst, followed by a rigorous evaluation of its performance. The comprehensive detection of the degradation rate of formaldehyde by  $\text{WO}_3$ -Cu,  $\text{WO}_3$ - $\text{CeO}_2$ , and  $\text{TiO}_2$  was carried out to demonstrate the catalytic effect of the catalyst. The test results showed that the  $\text{WO}_3$ -Cu photocatalyst outperformed other catalysts in terms of heat resistance, resistance to heavy metal pollution, stability, compressive strength, and anti-interference ability. Overall, the  $\text{WO}_3$ -Cu photocatalyst can improve the performance of various aspects of previous photocatalysts. However, this experiment only analyzed the catalytic effect of formaldehyde degradation, and whether this result applies to other catalytic reactions remains to be examined.

## R E F E R E N C E S

- [1] Nsugbe E. Toward a Self-Supervised Architecture for Semen Quality Prediction Using Environmental and Lifestyle Factors. *Artificial Intelligence and Applications*. 2023, 1(1): 35-42.
- [2] Ma C, Song W, Yang J, Ren C, Du H, Tang T, Cui H. The role and mechanism of commercial macroalgae for soil conditioner and nutrient uptake catalyzer. *Plant Growth Regulation*, 2022, 97(3): 455-476.
- [3] Hu X, Li X, Yang H, Xu C, Xiong W, Guo X, Zeng D. Active W sites promoted by defect engineering enhanced  $\text{C}_2\text{H}_6\text{S}_3$  sensing performance of  $\text{WO}_3$  nanosheets. *ACS sensors*, 2022, 7(7): 1894-1902.
- [4] Li T, Guo X, Zhang L, Yan T, Jin Z. 2D CoP supported 0D  $\text{WO}_3$  constructed S-scheme for efficient photocatalytic hydrogen evolution. *International Journal of Hydrogen Energy*, 2021, 46(39): 20560-20572.
- [5] Cai H, Ma Y, Li J, Jin Y, Zhu P, Chen, M. Norfloxacin degradation by persulfate activated with  $\text{Cu}_2\text{O}@\text{WO}_3$  composites: efficiency, stability, mechanism, and degradation pathway. *Industrial & Engineering Chemistry Research*, 2022, 61(30): 11237-11248.
- [6] Li S, Li Z, Li L, Dai X, Chen M, Zhu W.  $\text{TiO}_2$ - $\text{WO}_3$  loaded onto wood surface for photocatalytic degradation of formaldehyde. *Forests*, 2023, 14(3): 503-510.
- [7] Enesca A, Sisman V. Indoor air photocatalytic decontamination by UV-Vis activated  $\text{CuS/SnO}_2/\text{WO}_3$  Heterostructure. *Catalysts*, 2022, 12(7): 728-724.
- [8] Loka C, Lee K S. Dewetted silver nanoparticle-dispersed  $\text{WO}_3$  heterojunction nanostructures on glass fibers for efficient visible-light-active photocatalysis by magnetron sputtering. *ACS omega*, 2021, 7(1): 1483-1493.
- [9] Arslan M, Firat Y E, Tokgöz S R, Peksoz A H M E. Fast electrochromic response and high coloration efficiency of Al-doped  $\text{WO}_3$  thin films for smart window applications. *Ceramics International*, 2021, 47(23): 32570-32578.
- [10] Wang S, Li M, Ren L, Wu Y, Li L. Sensing performance for ethylene glycol of hydrothermally self-assembled 3D  $\text{WO}_3$ . *Ceramics International*, 2022, 48(13): 19206-19216.
- [11] Li Y, Cheng D, Wei Z, Sautet P. Photoelectron Storage at the  $\text{WO}_3/\text{TiO}_2$  Interface: Modeling in Ambient Conditions from First-Principles Calculations. *ACS Catalysis*, 2023, 13(15): 9979-9986.
- [12] Yang Z, Wang J, Wang J, Li M, Cheng Q, Wang Z, Zhang G. 2D  $\text{WO}_{3-x}$  nanosheet with rich oxygen vacancies for efficient visible-light-driven photocatalytic nitrogen fixation. *Langmuir*, 2022, 38(3): 1178-1187.

- [13] Shen F, Wang Z, Wang Y, Qian G, Pan M, Luo L, Yin S. Highly active bifunctional catalyst: Constructing FeWO<sub>4</sub>-WO<sub>3</sub> heterostructure for water and hydrazine oxidation at large current density. *Nano Research*, 2021, 14(11): 4356-4361.
- [14] Liu H, Wu H, Hu Z, Wang J, Wu Y, Yu H. One-side capping in two-dimensional WO<sub>3</sub>-type materials leading to strong second-harmonic response. *Chemistry of Materials*, 2022, 34(7): 3501-3508.
- [15] Kaur N, Zappa D, Maraloiu V A, Comini E. Novel christmas branched like NiO/NiWO<sub>4</sub>/WO<sub>3</sub> (p-p-n) nanowire heterostructures for chemical sensing. *Advanced Functional Materials*, 2021, 31(38): 2104416-2104420.
- [16] Eglitis R I, Purans J, Jia R. Comparative hybrid Hartree-Fock-DFT calculations of WO<sub>2</sub>-terminated cubic WO<sub>3</sub> as well as SrTiO<sub>3</sub>, BaTiO<sub>3</sub>, PbTiO<sub>3</sub> and CaTiO<sub>3</sub> (001) surfaces. *Crystals*, 2021, 11(4): 455-461.
- [17] Grigioni I, Di Liberto G, Dozzi M V, Tosoni S, Pacchioni G, Sellì E. WO<sub>3</sub>/BiVO<sub>4</sub> photoanodes: facets matching at the heterojunction and BiVO<sub>4</sub> layer thickness effects. *ACS Applied Energy Materials*, 2021, 4(8): 8421-8431.
- [18] Quyen V T, Kim J T, Park P M, Huong P T, Viet N M, Thang P Q. Enhanced the visible light photocatalytic decomposition of antibiotic pollutant in wastewater by using Cu doped WO<sub>3</sub>. *Journal of Environmental Chemical Engineering*, 2021, 9(1): 104737-104740.
- [19] Badour Y, Danto S, Labrugère C, Duttine M, Gaudon M. Cu-doped and un-doped WO<sub>3</sub> photochromic thin films. *Journal of Electronic Materials*, 2022, 51(4): 1555-1567.
- [20] Qi X, Gan J, Zhao Z, Li N, Chen Y, Jin T. Chitosan Sponge/Cu-WO<sub>3-x</sub> Composite for Photodynamic Therapy of Wound Infection. *Langmuir*, 2023, 39(7): 2631-2640.